Desalination with a Cascade of Cross-Flow Hollow Fiber Membrane Distillation Devices Integrated with a Heat Exchanger

Hanyong Lee, Fei He, Liming Song, Jack Gilron, and Kamalesh K. Sirkar
Otto H. York Dept. of Chemical, Biological and Pharmaceutical Engineering, Center for Membrane Technologies, New Jersey Institute of Technology, Newark, NJ 07102

DOI 10.1002/aic.12409
Published online October 19, 2010 in Wiley Online Library (wileyonlinelibrary.com).

Cost-efficient desalination technology was developed successfully by integrating a countercurrent cascade of the novel cross-flow direct contact membrane distillation (DCMD) devices and solid polymeric hollow fiber-based heat exchange devices. Simulations have been carried out for the whole DCMD cascade to project values of gained output ratio (GOR) as a function of the number of DCMD stages as well as other important factors in the cascade vis-à-vis the temperatures and flow rates of the incoming hot brine and cold distillate streams. The simulation results were verified with experimental results from cascades consisting of two to eight stages. The numerical simulator predicts a GOR of 12 when unequal flow rates of the incoming brine and distillate streams are used. An artificial sea water was concentrated eight times successfully when a countercurrent cascade composed of four stages of the DCMD modules and a heat exchanger was used during the DCMD process. © 2010 American Institute of Chemical Engineers *AIChE J,* 57: 1780–1795, 2011
Keywords: separation techniques, microporous membrane separations, evaporation, fibers, diffusion

Introduction

In direct contact membrane distillation (DCMD) process,[1,2] hot brine flows at atmospheric pressure on one side of a porous hydrophobic membrane and cold distillate flows on the other side of the membrane. Water vapor evaporated from the hot brine at the brine-membrane pore interface diffuses through the pores and is condensed at the pore-distillate interface on the other side of the membrane at a lower temperature. The water vapor pressure and, thus, the transmembrane flux increases exponentially with increasing temperature, while these are weak functions of salt concentration. Therefore, this thermal technique is relatively free from flux reduction by concentrating feed, which is inevitable in the reverse osmosis (RO)-based process. Consequently, the DCMD process is an appropriate alternative for achieving high water recovery from brackish/sea water feeds, managing the concentrate from desalination processes including RO, desalination in inland areas, and recovering water from industrial brines.[3]

We have recently developed a highly efficient hollow fiber cross-flow module for the DCMD process.[4] In a series of experiments with a single cross-flow DCMD module, it was shown to produce water vapor fluxes as high as 79 kg/(m^2 h) at the top feed temperature of 90°C.[5–7] This is due to the fact that the cross-flow arrangement of membrane fibers in a DCMD module reduces temperature polarization and thereby promotes both heat and mass transfer. In addition to the arrangement of brine flow vis-à-vis the hollow fibers arrangement, the novel highly porous fluorosilicone coating on porous

Correspondence concerning this article should be addressed to Kamalesh K.Sirkar at sirkar@adm.njit.edu.
Current Address of Hanyong Lee: R&D Center, Samsung Engineering Co. Ltd., Suwon, Kyounggi, Korea 443-823, ROK
Current Address of Liming Song: 3M corporation, St. Paul, MN
Current Address of Jack Gilron: Ben Gurion University, Beer-Sheva, Israel

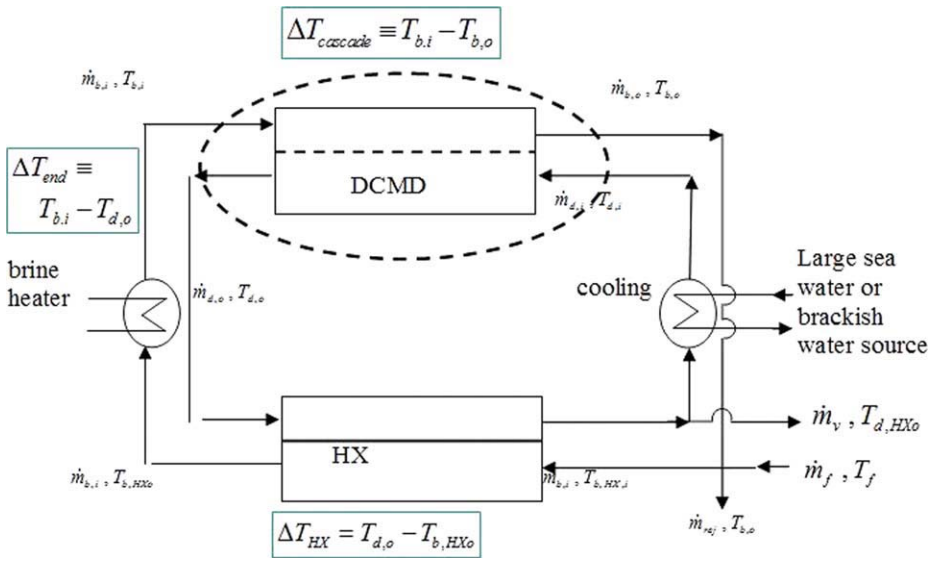

Figure 1. Countercurrent DCMD with heat recovery heat exchanger.

[Color figure can be viewed in the online issue, which is available at wileyonlinelibrary.com.]

polypropylene (PP) hollow fiber-based membranes showed strong resistance to scaling of $CaCO_3$ and $CaSO_4$.[8–10]

Although the principles of DMCD allow the process to be operated with waste heat such as low-grade steam, energetic optimization by heat recovery can extend the applicability of the process to the region where the waste heat is limited by quantity or no waste heat is available. Consideration on optimal heat recovery is also important when additional heat input is used to increase production with minimal impact on capital expenditure (CAPEX). Figure 1 illustrates the simplified process scheme of a countercurrent DCMD module integrated with a heat exchanger for energy recovery. The thermal energy carried by the distillate stream exiting the DCMD unit(s) is recovered to the feed brine. The feed, then, is heated up by an additional heat source to the top temperature, $T_{b,i}$. The heat duty of the additional heat source is proportional to the difference between the top feed temperature and the feed temperature exiting the heat exchanger, $T_{b,i}$, $T_{b,HX,o}$. This temperature difference can be broken up into two contributions: $\Delta T_{end} = T_{b,i} - T_{d,o}$ and $\Delta T_{HX} = T_{d,o} - T_{b,HX,o}$. In a countercurrent mode of operation, those two terms, ΔT_{end} and ΔT_{HX}, are dictated by the performance of the DCMD units and that of the heat exchanger, respectively. For example, the maximum heat recovery is achieved when $T_{d,o}$ is as close as possible to $T_{b,i}$ when the temperature difference across the heat exchanger is fixed (Figure 2). Note that ΔT_{end} is governed by the effective surface area of the given DCMD modules, which implies larger number of units in a cascade to obtain smaller ΔT_{end}. Also, note that ΔT_{end} is proportional to the driving force for the flux at the end of DMCD units, which implies that increasing the number of units decreases the average flux of entire DCMD units. Therefore, DCMD process development requires consideration of the trade-off among the heat duty, membrane flux, and surface area. Such general observations on the role of heat recovery in a DCMD process can be found in the literature.[11–13]

To realize such a countercurrent mode with cross-flow DCMD modules, a cascade arrangement integrated with heat exchanger must be studied. For such a system, Gilron et al.[3] considered the trade-off between the CAPEX, which is proportional to the membrane and the heat exchanger areas and the operating expenditure (OPEX) associated with the feed top temperature and heat duty. They presented a simplified

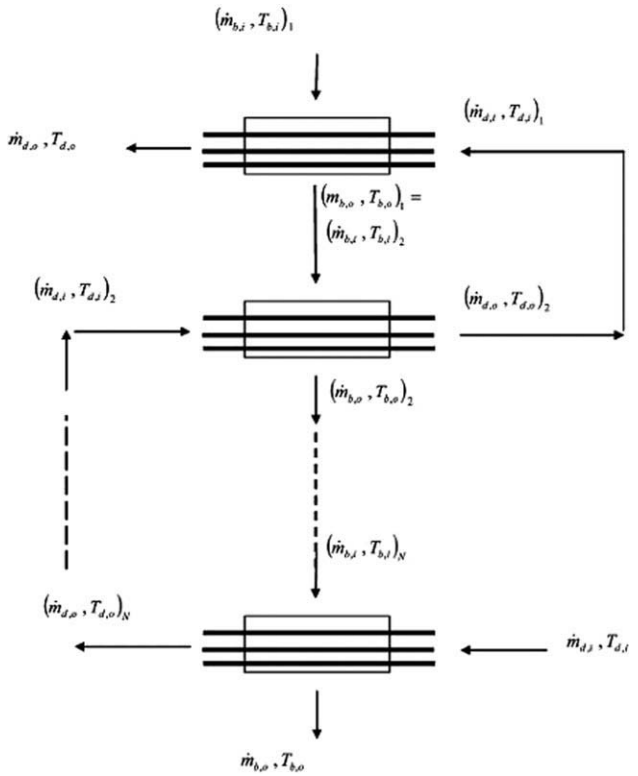

Figure 2. Scheme for using cross-flow DCMD modules to obtain a countercurrent cascade.

design method to determine the cost and performance of a cascade of cross-flow DCMD model-based process considering heat recovery.

This work is focused on experimentally studying a countercurrent cascade of cross-flow DCMD membrane modules in conjunction with a heat recovery heat exchanger. Experiments involved cascades with different stages at different temperatures. Simultaneously, a detailed simulation program has been developed to describe the observed behavior. The experiments have been carried out primarily with tap water as the brine. Model simulations to describe these experimental results have therefore used vapor pressure of pure water. Experiments have also been carried out using artificial sea water containing scaling salts such as $CaSO_4$ and $CaCO_3$; the system performance was explored when such a sea water was concentrated as much as eight times. Modeling of the DCMD devices required an estimation of the effective water vapor mass transfer coefficient k_m. This was also developed in experiments using small temperature differences between the hot brine and the colder distillate. In addition, simulations have been carried out for the whole DCMD cascade to project values of gained output ratio (GOR) as a function of the number of DCMD stages as well as other important factors in the cascade vis-à-vis the temperatures and flow rates of the incoming hot brine and the cold distillate streams.

Modeling of DCMD Cascade and Heat Recovery

Extension of modeling results is used to obtain the GOR as a function of the number of modules in a cascade, which together project the economics of the process. The GOR is a dimensionless number and defined as a ratio of the equivalent heat of produced water and the amount of heat supplied as follows:

$$\begin{aligned}
\mathrm{GOR} &= \frac{\dot{m}_v \cdot \Delta H_v}{\dot{m}_{bi} \cdot C_p \cdot (T_{b,i} - T_{b,HX,o})} = \frac{R \cdot \Delta H_v}{C_p \cdot (\Delta T_{end} + \Delta T_{HX})} \\
&= \eta \cdot \frac{\dot{m}_{bi} \cdot H_{b,i} - \dot{m}_{bo} \cdot H_{b,o}}{\dot{m}_{bi} \cdot C_p \cdot (T_{b,i} - T_{b,HX,o})} \\
&= \eta \cdot \frac{\dot{m}_{bi} \cdot C_p \cdot (T_{bi} - T_o) + \dot{m}_{bi} \cdot H_o - \dot{m}_{bo} \cdot C_p \cdot (T_{bo} - T_o) - \dot{m}_{bo} \cdot H_o}{\dot{m}_{bi} \cdot C_p \cdot (T_{b,i} - T_{b,HX,o})} \\
&= \eta \cdot \frac{\dot{m}_{bi} \cdot C_p \cdot T_{bi} - \dot{m}_{bi} \cdot C_p \cdot T_{bo} + \dot{m}_{bi} \cdot H_o - \dot{m}_{bo} \cdot H_o + \dot{m}_{bo} \cdot C_p \cdot T_o - \dot{m}_{bi} C_p \cdot T_o}{\dot{m}_{bi} \cdot C_p \cdot (T_{b,i} - T_{b,HX,o})} \\
&\cong \eta \cdot \frac{\dot{m}_{b,i} \cdot C_p \cdot T_{b,i} - \dot{m}_{b,o} \cdot C_p \cdot T_{b,o}}{\dot{m}_{b,i} \cdot C_p \cdot T_{b,i} - \dot{m}_{b,i} \cdot C_p \cdot T_{b,HX,o}} \cong \eta \cdot \frac{\Delta T_{cascade}}{\Delta T_{end} + \Delta T_{HX}} = \eta \cdot \frac{T_{b,i} - T_{b,o}}{T_{b,i} - T_{b,HX,o}},
\end{aligned} \tag{1}$$

where

$$\Delta T_{cascade} = T_{b,i} - T_{b,o} \tag{2}$$

$$\Delta T_{end} = T_{b,i} - T_{d,o} \tag{3}$$

$$\Delta T_{DCMD} = (T_{b,i} - T_{d,o})_{DCMD} \tag{4}$$

$$\Delta T_{HX} = T_{d,o} - T_{b,HX,o} \tag{5}$$

$$\text{Fractional recovery} = R = \frac{\dot{m}_v}{\dot{m}_{b,i}};\ \text{fractional recovery}\% = R \times 100\% \tag{6}$$

$$\eta \equiv \frac{\text{heat transfered from hot brine to cold distillate by mass transfer}}{\text{total heat transferred from hot brine to cold distillate}} \tag{7}$$

All calculations for GOR via Eq. 1 use only the first two relations in line 1 of Eq. 1; the relation in line 3 of Eq. 1 assumes that the reference state specific enthalpies of the brine inlet stream and the brine exit stream are identical. If we now assume that $\dot{m}_v \ll \dot{m}_{b,i}$ (i.e., the fractional recovery per pass is very small around 0.02–0.06), then the first relation in line 5 follows from that in line 4; the same assumption leads to the last two relations in line 5. Our ultimate objective is to arrive at these last two relations because they are very useful approximations for illustrative discussion valid for $\dot{m}_v \ll \dot{m}_{b,i}$, which is valid for all desalination studies conducted here. More importantly, this allows making explicit the connection between the brine-side temperature drop and the GOR, which is important in appreciating the results of cascade simulations.

Simulation of a DCMD Module

A DCMD cascade simulation program was developed based on a single DCMD module program described in Ref. [6]. We briefly summarize the model of the single DCMD module here. The mathematical model simulates the DCMD process in a single membrane module, where the hollow fiber membranes are all identical and present in a staggered arrangement (Figure 3). In each DCMD module, the brine flows on the shell side perpendicular to the hollow fiber axis; the distillate flows in the fiber lumen. When each stream enters a module, it is at a uniform temperature and is evenly distributed. No mixing of the brine is assumed between the fibers and the fiber layers in a DCMD module. Because of the heat and mass transfer through the membrane wall, the hot brine

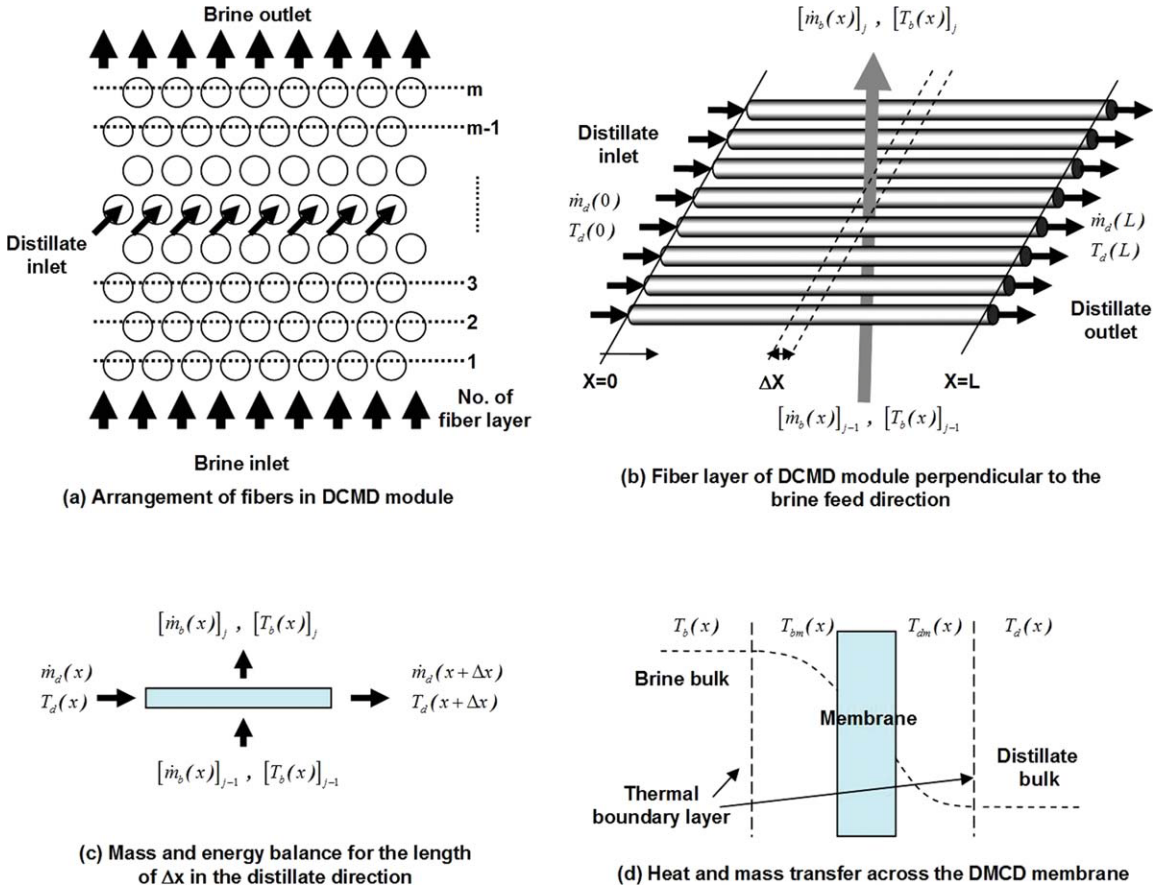

Figure 3. Setup for simulation of cross-flow DCMD module operation.

[Color figure can be viewed in the online issue, which is available at wileyonlinelibrary.com.]

flowing through the outside of fibers gets colder as it proceeds to the last layer of fibers, whereas the temperature of the cold distillate increases as it runs through the fibers. The vapor flux through the porous membrane is assumed to be proportional to vapor pressure difference between the brine and the distillate on two sides of the membrane wall.

In this model,[6] the heat fluxes with respect to the tube side membrane surface area in the jth fiber layer at location x along the fiber for the brine and distillate sides are given by:

$$\frac{1}{\alpha}\left(\frac{dQ(x)}{dx}\right)_j = h_{\mathrm{d}} A_{\mathrm{rd}} \left(T_{\mathrm{dm}}(x) - T_{\mathrm{d}}(x)\right)_j \qquad \text{distillate side} \quad (8)$$

$$\frac{1}{\alpha}\left(\frac{dQ(x)}{dx}\right)_j = h_{\mathrm{b}} A_{\mathrm{rb}} \left(T_{\mathrm{b}}(x) - T_{\mathrm{bm}}(x)\right)_j \qquad \text{brine side.} \quad (9)$$

The shell-side film heat transfer coefficient is taken from the Zukauskas correlation,[14] which was found to hold for cross flow on the shell side of membrane distillation units operated in vacuum mode.[5] The tube-side film heat transfer coefficient is the asymptotic value of the Nusselt number for fully developed thermal boundary layer. In hollow fiber heat exchangers, it has been shown to better approximate the actual heat transfer coefficient than the Seider-Tate correlation[15] and is also supported by the simulations of Ref. 16.

For heat transfer through the porous membrane, the total heat flux is given by contributions from both conduction and mass transfer-mediated enthalpy convection, which can be defined at the fiber lumen boundary[17]:

$$\frac{1}{\alpha}\left(\frac{dQ(x)}{dx}\right)_j = h_{\mathrm{m}} A_{\mathrm{r\,ln}} \left(T_{\mathrm{bm},j}(x) - T_{\mathrm{dm},j}(x)\right) + N_{\mathrm{v},j}(x) A_{\mathrm{r\,ln}} \left(\Delta H_{\mathrm{v}}(T_{\mathrm{dm},j}) + C_{\mathrm{P},j} T_{\mathrm{dm},j}\right). \quad (10)$$

The heat transfer coefficient used for the porous membrane was the isostrain area average heat transfer coefficient commonly used by many investigators[12,18]:

$$h_{\mathrm{m}} = \varepsilon h_{\mathrm{mg}} + (1-\varepsilon) h_{\mathrm{ms}}. \quad (11)$$

The distillate flux equation with respect to the log mean area is given by:

$$N_{\mathrm{v},j}(x) = k_{\mathrm{m}} \left(p_{\mathrm{bm},j}(x) - p_{\mathrm{dm},j}(x)\right), \quad (12)$$

where k_{m} is the effective vapor mass transfer coefficient. As those experimental studies carried out for comparing to simulations used tap water as the brine feed, we can conveniently assume that the water vapor partial pressures $p_{\mathrm{bm},j}$ and $p_{\mathrm{dm},j}$ are essentially equal to the vapor pressures[7] given by the Antoine equation, as tap water salt content was only around 100 ppm. The mass balance and heat balances for

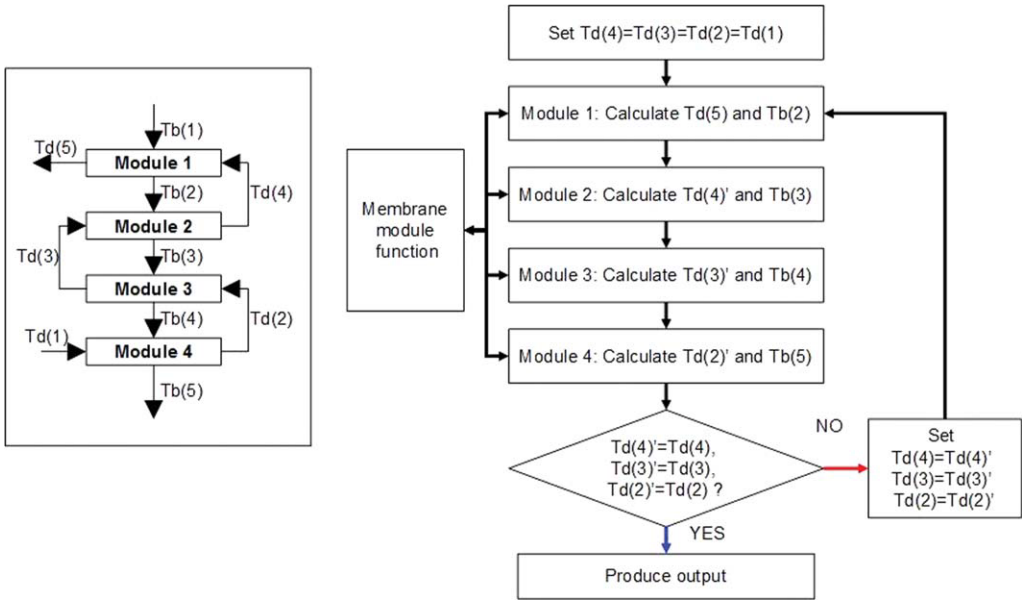

Figure 4. Calculation scheme for simulation of a cascade of four stages.

[Color figure can be viewed in the online issue, which is available at wileyonlinelibrary.com.]

each layer of the module along the distillate path and along the brine path are as given in Ref. 6.

A simulation program developed with MATLAB® to solve the model equations described above generated results, which were successfully verified by experiment.[6,7] This program was designed to produce outlet stream temperatures, a water production rate, and various parameters of interest for given inlet stream temperatures, inlet flow rates, and a value of k_m. In the next section, we will describe the development of the DCMD cascade simulation program by extending this simulation of a single DCMD module.

Simulation of a Cascade of Cross-Flow DCMD Modules

The extension of the above program to the multistage DCMD cascade was implemented using the single DCMD simulation program as a subfunction of the cascade simulation program. This hierarchical type of programing is convenient to explore many cases of DCMD module arrangements in a cascade, because it is not necessary to develop separate codes for different arrangements. The cascade simulation program calls the single-module DCMD simulator as a subfunction with input parameters such as inlet temperatures and flow rates of the brine and the distillate to calculate outlet temperatures and the production rate through a certain single module. Then, those calculation results of the single module were used as inputs for the calculation for the next stage. In other words, it assumes that the exit streams of the brine and the distillate from one stage are each completely mixed before each is introduced into the next stage of the DCMD module. Therefore, all assumptions used for developing the model of a single DCMD module still hold for the cascade simulation. As described in Figure 4 for the case of a four-stage cascade simulation, the iteration of calculation starts with the intermediate-stage temperatures of the distillate set to the distillate inlet temperature. After the calculation from the first stage to the last stage of the cascade with such an initial guess value, it produces a new set of intermediate temperatures of the distillate. Iterative calculation proceeds until these calculated intermediate temperatures and the used intermediate temperatures are close enough to satisfy the convergence criteria. The convergence of the numerical solutions was determined with a precision of 10^{-3}°C. The simulation code that realizes such numerical algorithm was developed with the script programing language of MATLAB®.

Table 1. Characteristics of DCMD Modules Used in DCMD Cascade Experiments

Membrane Modules #26–33*	
Fiber O.D. (μm)	630
Fiber I.D. (μm)	330
Membrane porosity	0.60
No. of fibers	$26 \times 29 = 754$
Effective fiber length (cm)	6.4
Effective internal membrane surface area† (cm^2)	500
Effective cross-sectional area for shell side liquid flow‡ (cm^2)	4.31

*Supplied by Applied Membrane Technologies, Minnetonka, MN.
†Based on fiber internal diameter (I.D.).
‡Based on open area for flow = frame cross-sectional area − No. of fibers in a layer × fiber O.D. × length of fiber.

Table 2. Characteristics of Heat Exchangers Used in DCMD Cascade Experiments

Polymeric Solid Hollow Fiber Heat Exchangers	HX1*	HX2*
Fiber O.D. (mm)	575	570
Fiber I.D. (mm)	425	430
No. of fibers	200	12,100
Effective fiber length (cm)	21.5	24
Effective fiber surface area† (cm^2)	574	39,230

*Supplied by Membrana, Charlotte, NC.
†Based on fiber internal diameter (I.D.).

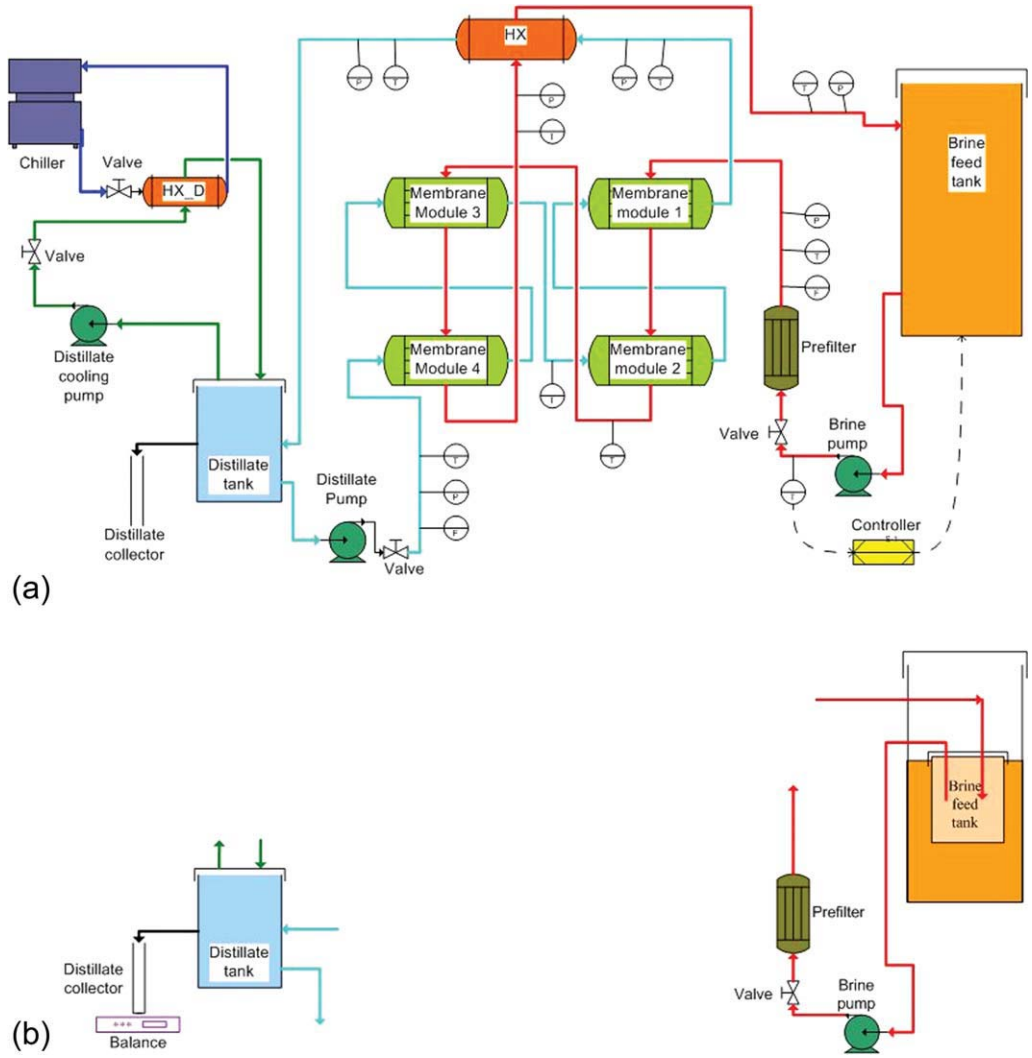

Figure 5. (a) Schematic diagram of experimental setup for DCMD-HX network with four membrane modules and one heat exchanger: an earlier experimental setup for the countercurrent cascade of cross-flow hollow fiber membrane modules; (b) modification of the experimental setup in Figure 5a vis-à-vis the brine feed tank and the distillate tank for the countercurrent cascade of cross-flow hollow fiber membrane modules.

[Color figure can be viewed in the online issue, which is available at wileyonlinelibrary.com.]

Experimental Study of DCMD Cascade and Heat Recovery

Membranes, modules, and heat exchangers

Each cross-flow rectangular hollow fiber membrane module had 12 fibers/layer and 13 layers of hollow fibers. In this membrane module, PP hollow fiber membranes (MEMBRANA, Wuppertal, Germany) coated on the O.D. with proprietary recipes by plasma polymerization at Applied Membrane Technology (AMT, Minnetonka, MN) were potted in a staggered manner; the coating was also quite porous. The physical properties and characteristic dimensions of the hollow fiber membranes and membrane modules as picture frames are listed in Table 1. The details of the shell-side entrance to and exit from the rectangular membrane modules designed and built at New Jersey institute of Technology (NJIT) to facilitate uniform flow perpendicular to the fibers in the rectangular module are described in Refs. 4 and 5. Two heat exchangers (HX1 and HX2) were obtained from Membrana, Charlotte, NC. The heat exchangers were built out of solid polypropylene hollow fibers. The dimensions of these fibers and the heat exchanger characteristics are provided in Table 2.

Experimental setup

A schematic of the experimental setup is shown in Figure 5a. Tap water and deionized water were used in this setup as the brine and the distillate, respectively. Hot brine in the feed tank was introduced into the membrane modules by a magnetic pump (MDX-1/2, March Mfg., Glenview, IL) through a prefilter (5 μm, 01508-30, US Filter, Sheboygan, WI), which removed any particles in the feed. Figure 5b shows the change in the brine tank section of the experimental setup, when using scaling salt solutions as the brine, to prevent fast deposition of scaling salts onto the heating coil

Table 3. Composition of an Artificial Sea Water

Sodium chloride	23.96 g/l
Magnesium chloride	5.08 g/l
Sodium sulfate	3.99 g/l
Calcium chloride	1.12 g/l
Potassium chloride	0.67 g/l
Sodium bicarbonate	0.2 g/l

in the brine tank shown in Figure 5a. The brine solution was now separated from the heating coil and was heated up by the water bath outside the brine feed tank, while the heating coil was immersed in the outside water bath. Consequently, a peristaltic pump (Masterflex, Cole-Parmer, Vernon Hills, IL) took the place of the magnetic pump to pump the hot brine into the shell side of the membrane modules. The prefilter cartridge was made of polypropylene with 1 μm in pore size (01512-00, Cole-Parmer, Vernon Hills, IL). The temperature of the brine feed was controlled and maintained by a PID temperature controller (89000-15, Cole-Parmer Instrument, Vernon Hills, IL) connected to the heating coil (492-6S, George Ulanet, Newark, NJ) immersed into the feed solution in the feed brine tank. The feed flow rate was controlled by a valve and measured by a rotameter (32250-12 and 94788-11, Cole-Parmer, Vernon Hills, IL). After passing through the shell sides of membrane modules in series, the brine was allowed to go through the shell side of the heat exchanger and then returned to the feed tank for heating and recycling.

A chiller (12 kW, CH3002A, Remcor® Product, Glendale Heights, IL) equipped with a pump controlled the temperature of the cold distillate. As the chiller had a limitation in dealing with high temperature, indirect temperature control of the distillate by coupling the distillate and the cold water from the chiller provided a wider range of choice for the distillate inlet temperatures. This was done using a separate heat exchanger (HX_D in Figure 5a). This polymeric solid hollow fiber-based heat exchanger was installed in a separate flow loop between the chiller and the distillate tank. In this way, the temperature of the distillate in the distillate tank was controlled by manipulating the temperature setting of the chiller and flow rate of the distillate through the heat exchanger. The distillate tank had another flow loop incorporating the membrane modules and the heat exchanger (HX1 or HX2). A valve between the distillate tank and the lumen side of the membrane module 4 (Figure 5a) was used to control the distillate feed flow rate measured by a digital flow meter (S-111-8, McMillan, Georgetown, TX). The distillate was allowed to flow through the lumen sides of the membrane modules with the hot brine in cross flow on the shell side of the membranes. The distillate passing through the lumen side of all membrane modules was circulated back to the distillate tank through the heat exchanger (HX1 or HX2). This heat exchanger allowed heat recovery from the hot distillate to the cold brine from the last membrane unit.

Table 4. Effects of the Heat Transfer Surface Area of the Heat Exchanger on Heat Recovery (T in °C)

Heat Exchanger	$T_{b,i}$	$T_{d,o}$	$T_{b,HX,o}$	$T_{d,HX,o}$	$T_{b,o}$	$T_{d,i}$
HX1	80	67	49.4	59.5	41.6	33.9
HX2	80.1	68	65.5	48.6	44.7	37.7

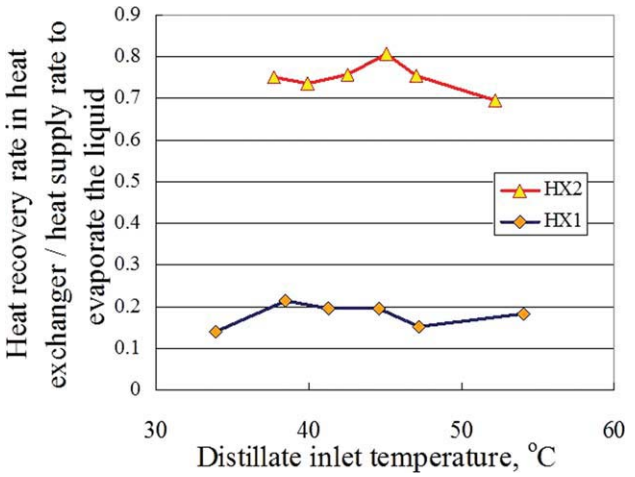

Figure 6. Heat recovery rate in heat exchanger divided by heat supply rate to evaporate the liquid for heat exchangers HX1 (surface area = 574 cm^2) and HX2 (surface area = 39,230 cm^2) as a function of distillate inlet temperature in a four-stage DCMD cascade.

[Color figure can be viewed in the online issue, which is available at wileyonlinelibrary.com.]

The inlet and outlet temperatures of the membrane module cascade and the heat exchanger for both the brine and the distillate were measured by thermocouples (the inlet temperatures of the heat exchanger were assumed to be equal to the outlet temperatures of the membrane modules at the last stage). As these DCMD experiments had both heat transfer and mass transfer, all piping and the prefilter were insulated to drastically reduce heat loss to the surrounding. The pressure drops of the brine feed and the distillate through the membrane modules were also monitored. The distillate production rate was measured by collecting the overflow from the distillate tank. An electronic balance (ACB-plus 1500, Adam, UK) was used here to measure continuously the accumulated distillate and thus the water vapor production rate. The distillate conductivity was measured by a conductivity meter (Orion 115A+, Thermo Electron, Waltham, MA) to monitor for possible leaks across the membrane module or the heat exchanger.

Experimental procedure for feed brine containing scaling salts

The scaling salt-containing experiments were conducted with an artificial sea water. The composition of the artificial sea water included major ions in sea water, such as Na^+, Mg^{2+}, K^+, Ca^{2+}, Cl^-, SO_4^{2-}, and HCO_3^-. The specific data are listed in Table 3.[19] The feed solution of artificial sea water was prepared as follows: NaCl, $MgCl_2$, $CaCl_2$, and KCl were dissolved together in tap water; Na_2SO_4 and $NaHCO_3$ were prepared together in tap water. Before the two solutions were mixed in the brine tank, each was stirred sufficiently to make sure each chemical was dissolved.

The concentration times of the artificial sea water was calculated by the ratio of original feed volume to the difference between the original feed volume and the overall volume of

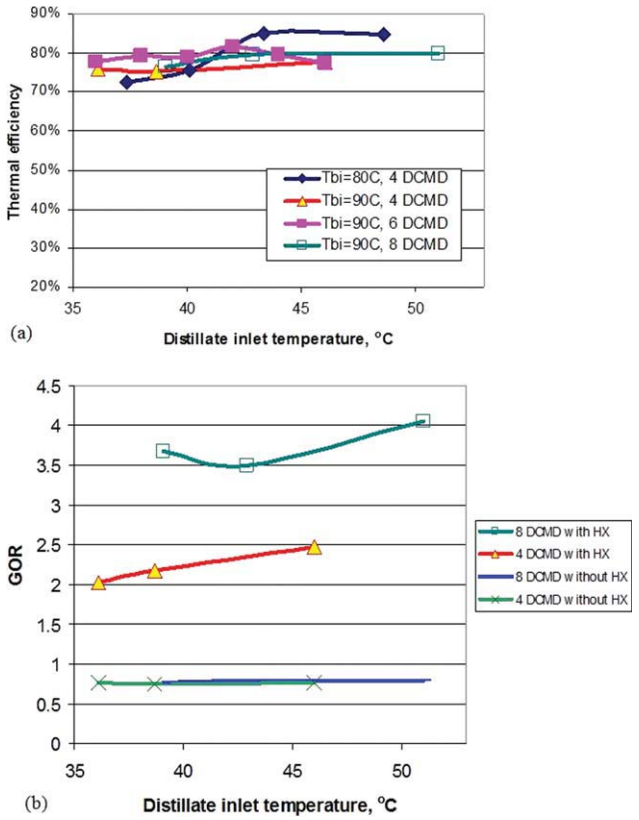

Figure 7. Experimental results of (a) thermal efficiency and (b) GOR as a function of the distillate inlet temperature for equal inlet flow rates of the brine and the distillate at 0.5 l/min ($T_{b,i}$ = 90°C).

[Color figure can be viewed in the online issue, which is available at wileyonlinelibrary.com.]

distillate produced during the DCMD process. Other parameters tested include the pH value and the calcium ion concentration in the brine solution, as described in Refs. 8–10.

The scaling potential of $CaSO_4$ or $CaCO_3$ in the artificial sea water was evaluated via the saturation index (SI), which is defined for a salt of formula $M_{v+}\,X_{v-}$ as follows[20]:

$$\mathrm{SI} = \frac{a_{\mathrm{M}}^{v+} a_{\mathrm{X}}^{v-}}{K_{\mathrm{SP}}^{0}} = \frac{[\mathrm{M}]^{v+}[\mathrm{X}]^{v-}}{K_{\mathrm{SP}}} \left(\frac{\gamma_{+/-}}{\gamma_{+/-,\mathrm{eq}}}\right)^{v} :$$

$$K_{\mathrm{SP}} = [\mathrm{M}]_{\mathrm{eq}}^{v+}[\mathrm{X}]_{\mathrm{eq}}^{v-}. \qquad (13)$$

Once calcium sulfate or calcium carbonate precipitation had occurred, it was then possible to determine if such precipitation had any effect on the performance of the DCMD module vis-à-vis the water vapor flux, distillate contamination, and pressure drop.

Experimental Results and Discussion

Effects of heat exchanger on the heat recovery

Table 4 compares the steady-state temperatures when different heat exchangers (Table 2) were used for heat recovery. Here, four membrane units were put in a countercurrent cascade, and the hot brine and the cold distillate were introduced at 0.5 l/min. A steady state was assumed if there were no apparent changes in temperatures for more than 30 min. Although very similar temperatures of brine inlet (80°C) and distillate inlet (34 or 38°C) for both experiments resulted in apparently close brine temperatures at the exit from four DCMD stages ($T_{b,o}$), the brine exiting from the heat exchanger had a much higher temperature ($T_{b,HX,o}$) when it recovered energy through the larger heat exchanger HX2; this illustrates higher heat recovery with a higher heat exchanger area.

Figure 6 illustrates the rate of heat recovery by the brine from the distillate stream exiting the DCMD cascade, when using two different heat exchangers, as a function of the distillate inlet temperature for a fixed total membrane area (2000 cm^2 = 500 cm^2/stage × 4 stages) and a fixed brine inlet temperature (80°C). As expected, it shows that the larger surface area of the heat exchanger, HX2, allowed higher energy recovery from the distillate so that over 70% of the energy required for evaporation was recovered.

As shown in Figure 7a, the thermal efficiency of the membrane modules varied between 0.73 and 0.87 over the range of the experimental conditions studied. These high values show the improved thermal efficiency achieved by a countercurrent cascade compared to that when a single module was exposed to a much higher temperature gradient.[4] The GOR, shown in Figure 7b, reached a value of about 4.1 for eight DCMD modules in a cascade, a brine inlet temperature of 90°C, and equal inlet flow rates of the brine and the distillate (=0.5 l/min). There are two reasons for a lower GOR: equal flow rates of brine and distillate as we will see in the Section entitled "Maximizing GOR with operating parameters" and possible heat loss to the surrounding especially in the heat exchanger. Without the heat recovery, GOR cannot be more than 1. The temperature difference between $T_{d,o}$ and $T_{b,HX,o}$ varied between 3 and 7°C. A higher GOR is expected when the heat exchanger(s) reduces the value of $T_{d,o} - T_{b,HX,o}$. Therefore, focusing on the achievement of an energy-efficient DCMD process, the simulation study has been conducted assuming that $T_{d,o} - T_{b,HX,o}$ is 2°C.

Experimental Verification of the DCMD Cascade Model Predictions

In the simulation study, our goal was to find operating conditions of the DCMD process such as the number of stages in a cascade, inlet temperatures, flow rates, etc. to achieve higher

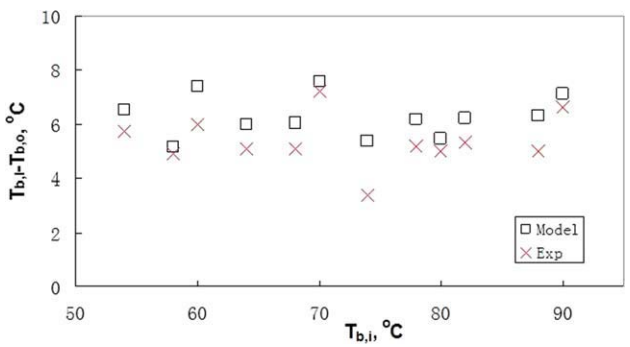

Figure 8. Experimental and modeling results for a two-stage cascade DCMD process with $T_{b,i} - T_{d,i}$ = 7–10°C and equal flow rates of the brine and the distillate (=0.5 l/min).

[Color figure can be viewed in the online issue, which is available at wileyonlinelibrary.com.]

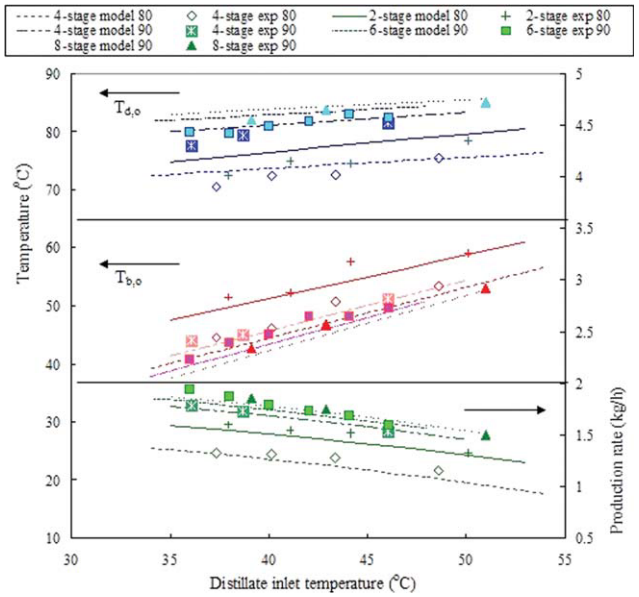

Figure 9. Comparison of outlet temperatures and production rates between modeling and experimental results for cascades (from two to eight stages) with $T_{b,i}$ = 80 or 90°C and equal incoming flow rates of brine and distillate = 0.5 l/min.

The "exp" and "model" in the legends represent experimental results and modeling results, respectively; "80" and "90" refer to $T_{b,i}$ = 80°C and $T_{b,i}$ = 90°C, respectively. [Color figure can be viewed in the online issue, which is available at wileyonlinelibrary.com.]

GOR. Experimental results of the steady-state temperatures and production rate have been used to verify the simulation results. These will be presented in this section.

The local mass-transfer coefficient in a membrane module depends on both the thermal conditions creating the driving force of the vapor pressure difference across the membrane and the complex local fluid flow pattern. These conditions will vary with the location in the DCMD module. However, it was found earlier that the simulator for a single DCMD module predicted the experimental results reasonably well for a constant membrane mass transfer coefficient, k_m, of 0.0024 kg/(m^2 h Pa) over the range of study.[6] Note that the temperature increase (for the distillate) or decrease (for the brine) in a multistage DCMD cascade is expected to be larger than that in a single DCMD module if the same flow rates are used. Therefore, it is still necessary to verify whether this constant value still holds true for the wider spectrum of the temperatures encountered in a multistage DCMD cascade. In other words, if the temperature variation over the entire membrane surface area is small, the local mass transfer coefficient at any location will be likely to be close to the overall mass transfer coefficient.

Two-stage cascade experiments were conducted to investigate the variation if any in the membrane mass transfer coefficient with a variation in inlet temperatures. To produce a measurable quantity of water vapor, the temperature difference between the brine inlet and the distillate inlet was maintained in the range of 7–10°C for all experiments. As shown in Figure 8, the modeling results for the difference between the brine inlet and the brine outlet temperature calculated using the constant membrane mass transfer coefficient of 0.0024 kg/(m^2 h Pa) describe the experimental data reasonably well over the entire range of the studied hot brine inlet temperature (54–90°C). This implies that it is safe to use the constant value of the overall membrane mass transfer coefficient in the simulation of a DCMD cascade. The model predicted a higher difference $T_{b,i} - T_{b,o}$ in the range of 0.5–1.5°C; most of them are around 1°C. Thermal losses do reduce the experimental flux and lead to less drop in brine temperature.

Other experiments with a cascade of two to eight stages for $T_{b,i}$ = 80 or 90°C were conducted to verify the modeling results. The outlet temperatures of brine/distillate and also the water vapor production rates were compared with the modeling results, as illustrated in Figure 9. In spite of the various operating conditions studied, the errors in the predicted outlet temperatures are less than 2°C, and those of the predicted production rates are less than 0.05 kg/h (or 3.5% of experimental data). It should be mentioned that there were also fairly small overprediction of distillate outlet temperature and underprediction of brine outlet temperature as the model of the single DCMD module does. One reason might be that the developed DCMD cascade simulation program uses the single DCMD model for each stage. Probably, the asymptotic Nusselt number, which is somewhat higher near the entrance of each module, is responsible for such systematic errors, and a more detailed computational fluid dynamics-based calculation may be used to produce better results. Another reason is the heat loss of brine during the DCMD experiments especially in the large heat exchanger. Consequently, the experimental results show a little lower thermal efficiency and water recovery than the simulation results. All results indicate that both experimental and modeling results satisfy the energy and the mass balances very well in spite of the small difference between them.

Maximizing GOR with Operating Parameters

In this section, the model whose predictions were found to simulate the experimental results well will be used to investigate the behavior of the DCMD cascade integrated with heat exchange and to find conditions which maximize GOR. As shown in Figure 10, for equal inlet flow rates of the brine and the distillate, increasing the number of stages in a cascade makes the brine outlet temperature and the distillate outlet temperature approach increasingly the distillate inlet temperature and the brine inlet temperature, respectively. It is obvious because the surface area for mass transfer-based heat transfer in a cascade increases with the number of stages. Likewise, the fractional water recovery also increases with the number of stages in a cascade. The GOR consequently increases with the number of stages because of the lower values of the temperature of approach and the increasing water vapor production.

Similar effects can be obtained by decreasing the equal flow rates of $F_{b,i}$ and $F_{d,i}$. If one uses lower flow rates, the residence times of the brine and the distillate in the membrane modules increase. Therefore, $T_{d,o}$ approaches $T_{b,i}$, $T_{b,o}$ approaches $T_{d,i}$, and the fractional water recovery increases with decreasing flow rate. All effects lead to increasing GOR.

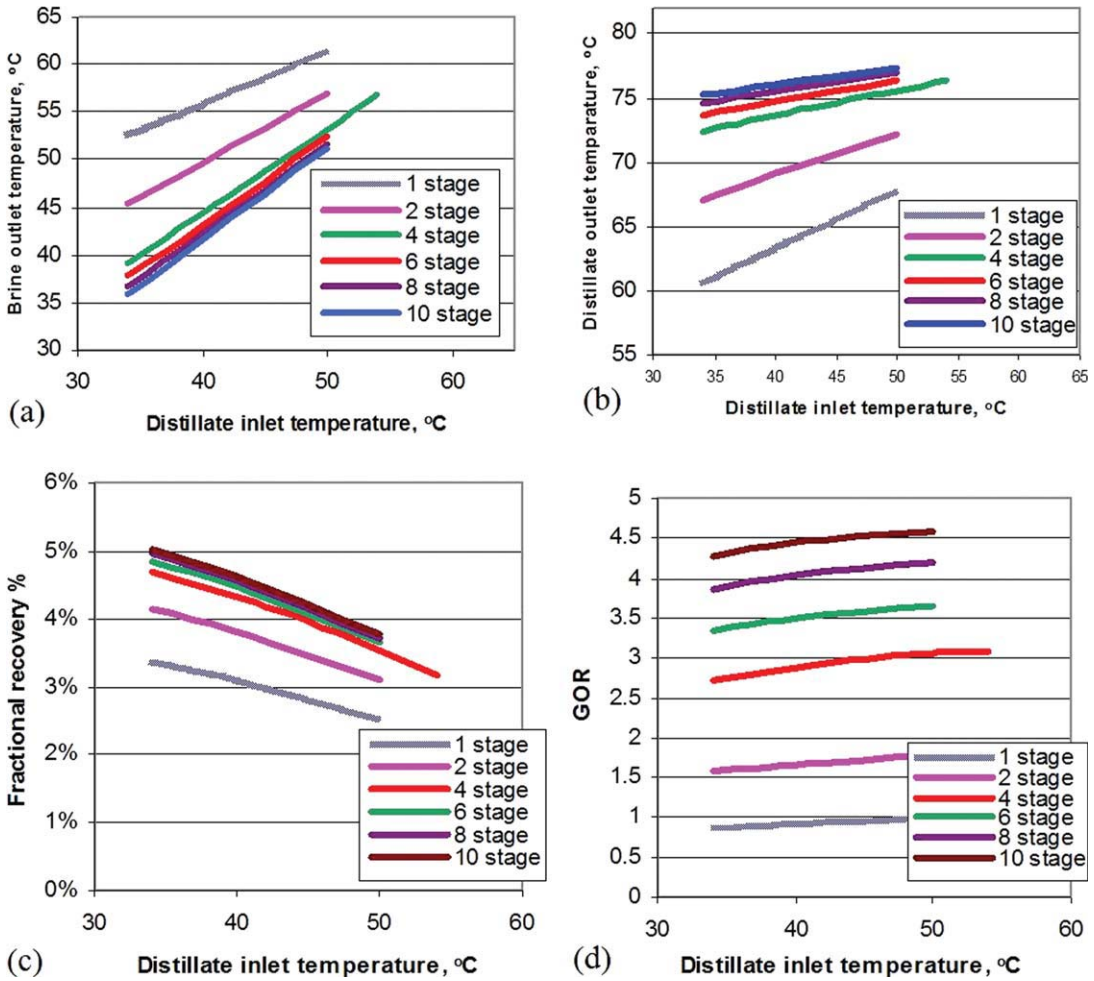

Figure 10. Modeling results for different stage numbers in a cascade with $T_{b,i}$ = 90°C and equal flow rates of brine and distillate = 0.5 l/min.

(a) Brine outlet temperatures; (b) distillate outlet temperature; (c) fractional water recovery; and (d) GOR for $\Delta T_{HX} = 2°C$. [Color figure can be viewed in the online issue, which is available at wileyonlinelibrary.com.]

The inlet temperatures of the brine and the distillate also affect GOR. If one increases the brine inlet temperature keeping the distillate inlet temperature constant, the vapor pressure difference applied across the membrane increases and the fractional water recovery increases. For example, when $T_{b,i}$ increases from 70 to 95°C, for various stage numbers of the membrane modules in the cascade from 2 to 10 ($T_{d,i} = 35°C$, $F_{b,i} = F_{d,i} = 0.5$ l/min, $\Delta T_{HX} = 2°C$), although the approach temperature, $\Delta T_{end} = T_{b,i} - T_{d,o}$, also increases for fixed membrane surface area, the dominant effect of the fractional water recovery on GOR leads to an increase of GOR. Similarly, decreasing the distillate inlet temperature for a fixed brine inlet temperature also increases the fractional water recovery and the approach temperature, $T_{b,i} - T_{d,o}$. In the case when $T_{d,i}$ decreases from 60 to 34°C, for various stage numbers of the membrane modules in the cascade from 2 to 10 ($T_{b,i} = 90°C$, $F_{b,i} = F_{d,i} = 0.5$ l/min, $\Delta T_{HX} = 2°C$), the approach temperature shows, however, more dominant effects on GOR and consequently GOR decreases with a decrease in the distillate inlet temperature. It is due to the fact that the water vapor pressure change gets smaller by decreasing the temperature of water. Effects of temperature on the fractional water recovery are quite small in the low temperature side. Figure 11 shows such an effect even more clearly. For this figure, DCMD cascade simulator was run with a constant $T_{b,i} - T_{d,i} = 55°C$. If one increases both brine inlet temperature and distillate inlet temperature, while keeping the $T_{b,i} - T_{d,i}$ constant, the predicted GOR increases mainly because of the increasing fractional recovery. Because of the exponentially increasing water vapor pressure with temperature, the choice of higher temperature values for the brine and the distillate leads to higher fractional water recovery.

From Figure 10, it should be noted that ΔT_{end} ($=T_{b,i} - T_{d,o}$) is always larger than $T_{b,o} - T_{d,i}$ for fixed inlet temperatures of brine and distillate. As $T_{d,o}$ imposes a limit on the highest temperature of $T_{b,HXo}$ after heat recovery, larger ΔT_{end} implies less possible amount of heat can be recovered. For equal inlet flow rates of the brine and the distillate, this particular trend can be explained by the following equation[3] with ΔT_{stage} in that reference replaced by $\Delta T_{cascade}$:

$$\left[T_{d,o} - T_{d,i}\right] = \frac{\dot{m}_{b,o}}{\dot{m}_{d,i}} \Delta T_{cascade} + \frac{\dot{m}_{v}}{\dot{m}_{d,i}} \Delta T_{end} \qquad (14)$$

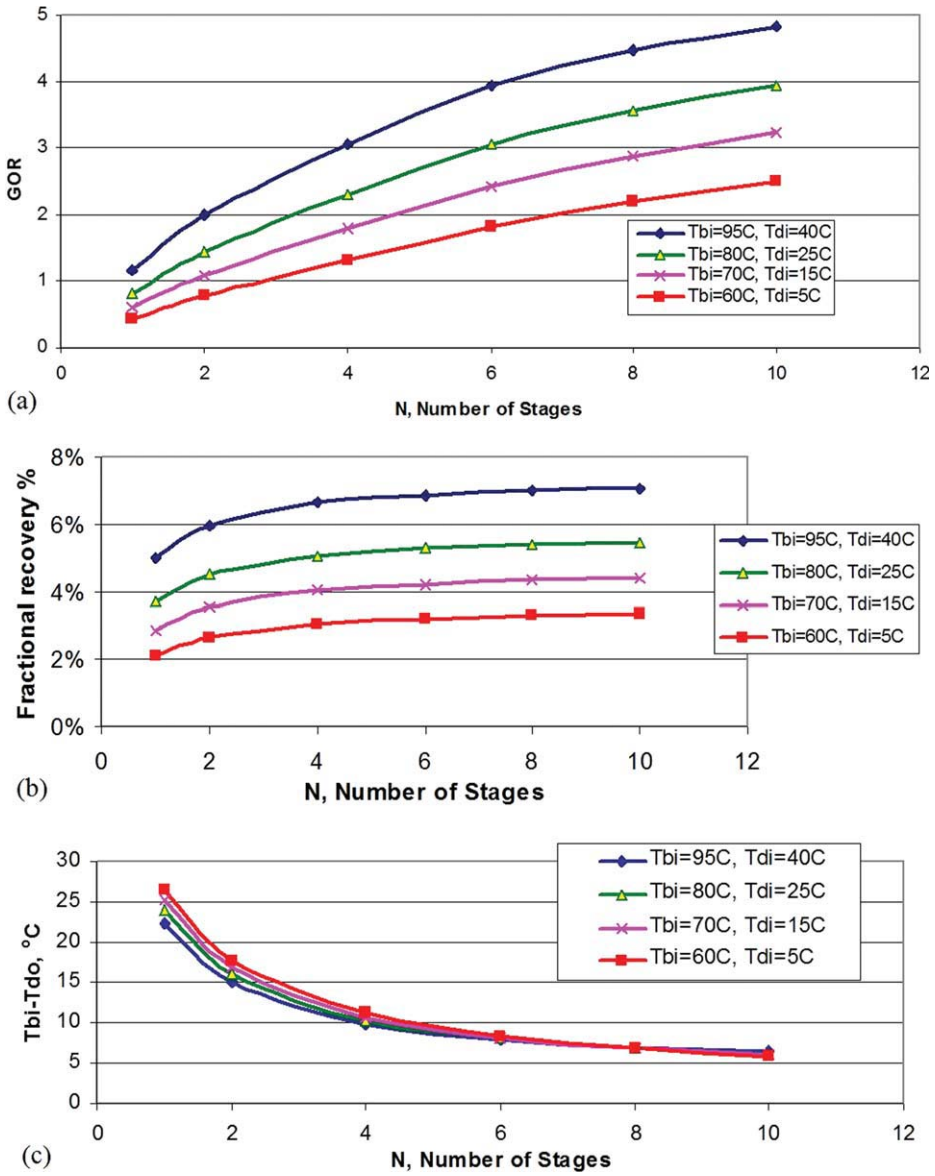

Figure 11. Modeling results for a four-stage cascade DCMD with $T_{b,i} - T_{d,i} = 55°C$ and equal flow rates of the brine and the distillate = 0.5 l/min.

(a) GOR for $\Delta T_{HX} = 2°C$; (b) fractional water recovery; and (c) temperature of approach $T_{b,i} - T_{d,o}$. [Color figure can be viewed in the online issue, which is available at wileyonlinelibrary.com.]

As $\Delta T_{cascade}$ $(= T_{b,i} - T_{b,o}) > \Delta T_{end}$ and $\dot{m}_{b,i} = \dot{m}_{d,i} = \dot{m}_{b,o} + \dot{m}_v$, for $\dot{m}_v > 0$, the following inequality holds:

$$\begin{aligned}\left[T_{d,o} - T_{d,i}\right] &= \frac{\left(\dot{m}_{d,i} - \dot{m}_v\right)}{\dot{m}_{d,i}}\Delta T_{cascade} + \frac{\dot{m}_v}{\dot{m}_{d,i}}\Delta T_{end} \\ &= \Delta T_{cascade} - \frac{\dot{m}_v}{\dot{m}_{d,i}}\left(\Delta T_{cascade} - \Delta T_{end}\right) \\ &< \Delta T_{cascade} = T_{b,i} - T_{b,o}. \end{aligned} \quad (15)$$

Therefore,

$$T_{d,o} - T_{d,i} < T_{b,i} - T_{b,o} \quad \text{or} \quad T_{b,i} - T_{d,o} < T_{b,o} - T_{d,i}. \quad (16)$$

The above inequality clearly shows that the distillate outlet temperature cannot approach the brine inlet temperature as much as the brine outlet temperature does to the distillate inlet temperature. This, in turns, implies that water production (or fractional water recovery) imposes a limitation to the heat recovery. Considering both heat recovery and water production in GOR, there should be a maximum of GOR.

Figure 12 shows such a variation of GOR as a function of the distillate inlet temperature and the number of stages in a cascade when the brine and the distillate are introduced into the cascade at the same flow rate (0.125 l/min). As the distillate inlet temperature approaches the brine inlet temperature, $T_{b,i} = 95°C$, ΔT_{end} and fractional recovery decrease, which results in GOR reaching a maxima at $T_{d,i} = 60°C$. For a fixed distillate inlet temperature, variation of ΔT_{end} with respect to number of stages in a cascade is somewhat larger than that of the fractional recovery. Therefore, ΔT_{end} plays a major role in varying GOR with

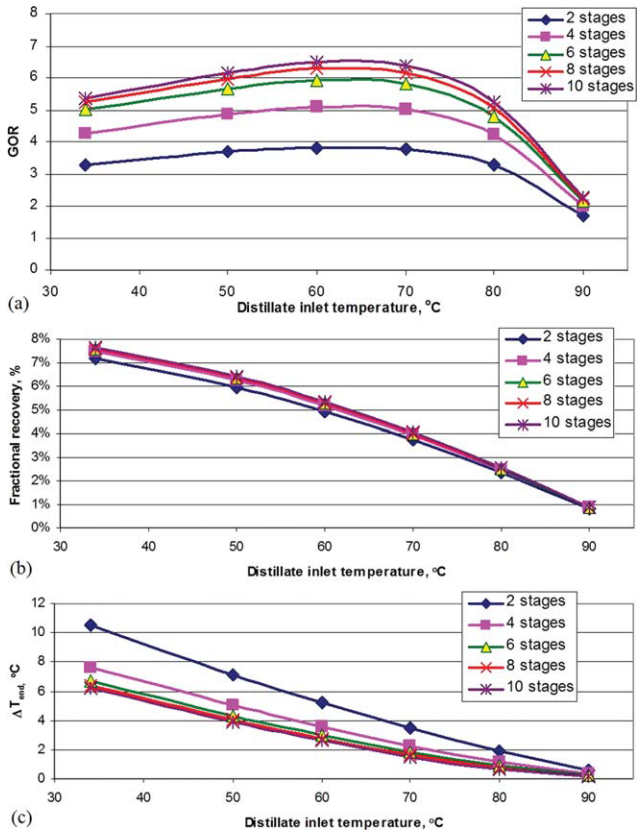

Figure 12. Modeling results of (a) GOR, (b) fractional recovery, and (c) ΔT_{end} as a function of distillate inlet temperature and number of stages, N, when $T_{b,i}$ = 95°C, ΔT_{HX} = 2°C, and equal incoming flow rates of the brine and the distillate = 0.125 l/min.

[Color figure can be viewed in the online issue, which is available at wileyonlinelibrary.com.]

respect to number of stages. Also, note that ΔT_{end} is still 2.6°C even for 10 stages, whereas $T_{b,o} - T_{d,i}$ is 0.6°C. It is due to the fact that water production decreases brine outlet flow rate and increases distillate flow rate. Balancing outlet flow rates of the brine and the distillate can even lower the ΔT_{end} for a fixed membrane area by minimizing the limitation of temperature approach imposed by water production.

Figure 13a shows that GOR significantly increases by such an approach. Introducing the brine inlet flow rate at a slightly higher level than the distillate inlet flow rate enough to compensate for the water production, which eventually increases the distillate outlet flow rate and decreases the brine outlet flow rate, results in a much smaller ΔT_{end}, which results in a GOR almost twice as large. For 10 stages and 6.67 $m^2/(m^3$ h) of the specific area based on the distillate, GOR reaches more than 12 and ΔT_{end} is as low as 0.6°C. It should be also noted that such significant improvement on GOR requires little sacrifice of the fractional recovery as shown in Figure 13b; only 0.2% decrease of the fractional recovery had taken place using a slightly higher flow rate of the brine. Obviously, ΔT_{end} can be even lower for the fixed number of stages by further increasing the flow rate of the brine. An experimental result for DCMD of an eight-stage cascade (in Figure 13c) shows that GOR could reach close to 6 when $F_{b,i}$ = 0.5 l/min, $F_{d,i}$ = 0.43 l/min, $T_{b,i}$ = 90°C, and $T_{d,i}$ = 42–50°C. (Higher values were not reached

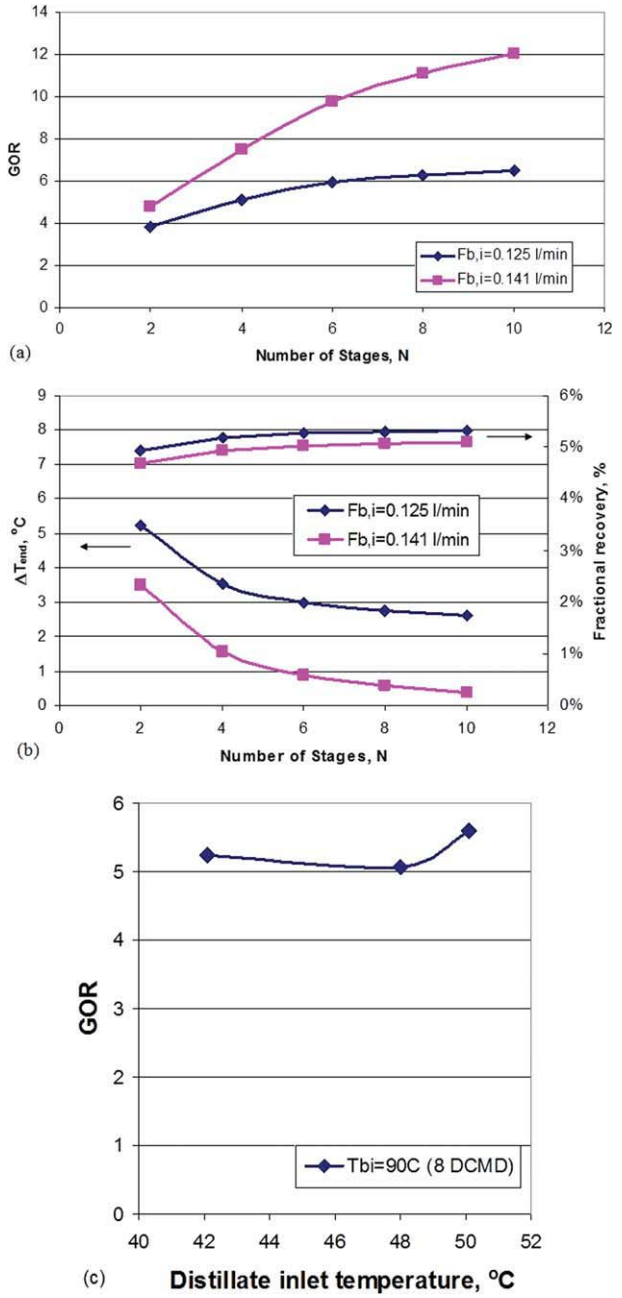

Figure 13. (a) Modeling results of GOR, (b) modeling results of fractional recovery and ΔT_{end}, as a function of distillate inlet flow rate and number of stages, N, when $T_{b,i}$ = 95°C, $T_{d,i}$ = 60°C, ΔT_{HX} = 2°C, and the inlet flow rate of the distillate = 0.125 l/min, (c) Experimental results of GOR vs. distillate inlet temperature for DCMD of an eight-stage cascade when $T_{b,i}$ = 90°C, inlet flow rate of brine = 0.5 l/min, and inlet flow rate of distillate = 0.43 l/min.

[Color figure can be viewed in the online issue, which is available at wileyonlinelibrary.com.]

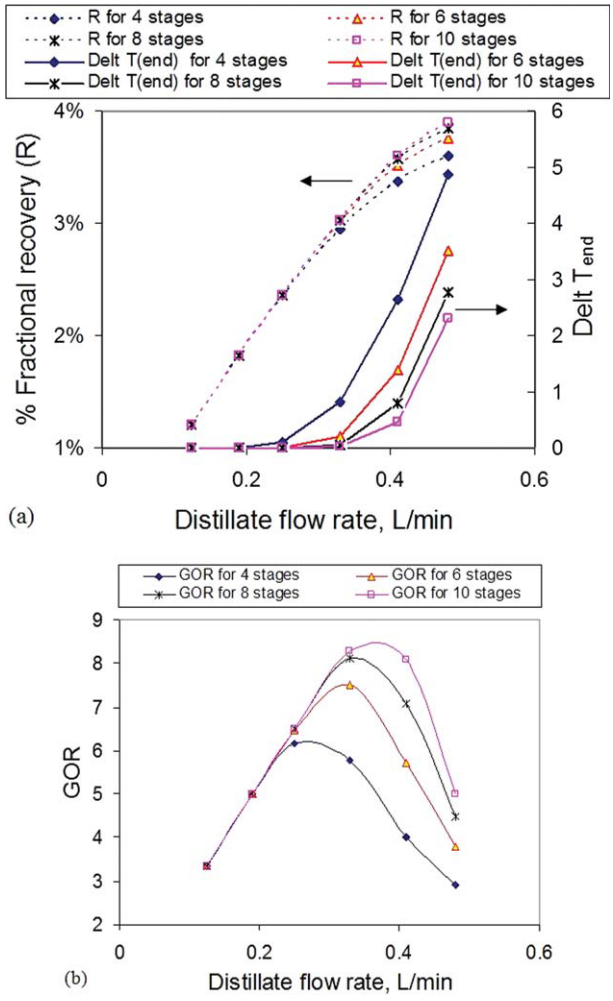

Figure 14. Simulation results on the fractional recovery and GOR vs. the distillate flow rate.

Here, $T_{b,i}$ = 78°C (brine inlet), $T_{d,i}$ = 44.8°C (distillate inlet), flow rate of brine = 0.5 l/min, and ΔT_{HX} = 2°C. [Color figure can be viewed in the online issue, which is available at wileyonlinelibrary.com.]

because of heat losses to the environment.) However, much higher inlet flow rate of the brine than that of the distillate causes significant drop of the fractional recovery, and consequently, it leads to a decrease of GOR.

For the case of different incoming flow rates of brine and distillate (here, $m_{b,i}$ = 0.5 l/min, $T_{b,i}$ = 78°C, $T_{d,i}$ = 44.8°C, and ΔT_{HX} on brine side is assumed to be 2°C), the simulated effects of distillate inlet flow rates on the fractional recovery and GOR are illustrated in Figure 14. They show that there is a maximum point of GOR in the curve of GOR vs. distillate flow rate for a variety of cascade stage numbers. The maximum value of GOR depends on the distillate flow rate. When the distillate flow rates are too low, the temperature difference between the brine inlet temperature and the distillate outlet temperatures is very close, which leads to a tiny difference in the water vapor pressure between the brine side and distillate side for part of the cross-flow hollow fiber membrane module. The direct result is that the water vapor flux is low leading to low fractional recovery, as shown in Figure 14a. When the distillate flow rate is higher, ΔT_{end} increases; with the increase of ΔT_{end}, the fractional recovery increases. This is similar to that for a single-stage DCMD. However, there are two stages for the change of both water recovery and ΔT_{end}. With the increase in the distillate flow rate, the water vapor recovery increase is slower, whereas ΔT_{end} increases faster. Because the GOR depends on both the water recovery and ΔT_{end} as shown in Eq. 1, there appears to be a maximum point for GOR. When the distillate flow rate is lower than 0.25 l/min, there is no difference in R or ΔT_{end} between cascades with different stages. Consequently, GOR shows no big difference for cascades with different stages when the distillate flow rate is lower than 0.25 l/min. When the distillate flow rate is higher than 0.25 l/min with the increase of stages in the cascade, the water vapor flux increases and ΔT_{end} decreases. Consequently, more stages in the cascade help to improve the GOR value. This trend of the dependence of GOR on the number of stages in the cascade is the same with the case in which the distillate and the brine have the same flow rates.

Concentrating Artificial Sea Water in a Countercurrent Cascade of DCMD Cross-Flow Modules

Saturation indices for gypsum, anhydrite, and calcite as functions of concentration times of artificial sea water at a temperature of 80°C are shown in Figure 15. The results were calculated using a thermodynamics simulation software (OLI StreamAnalyzer). This figure shows that the nucleation process for calcite might start at the beginning of the experiment as the SI value of calcite in the artificial sea water at 80°C is 3. The SI value of the calcite exhibits a maximum value of 12 at concentration factor of 6. For $CaSO_4$ in the hot feed, SI value for either gypsum or anhydrite keeps increasing with the concentration times. When the artificial sea water is concentrated eight times, the SI for gypsum and anhydrite is 2 and 6, respectively.

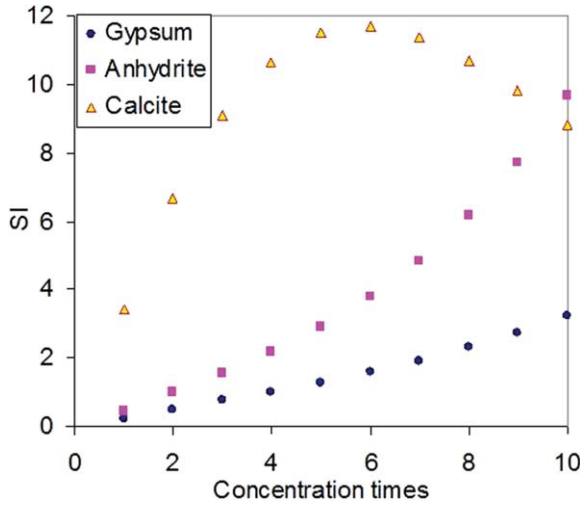

Figure 15. Saturation indices for gypsum, anhydrite, and calcite, respectively, vs. concentration times of artificial sea water at temperature = 80°C and pressure = 1 atm obtained from the software of OLI StreamAnalyzer.

[Color figure can be viewed in the online issue, which is available at wileyonlinelibrary.com.]

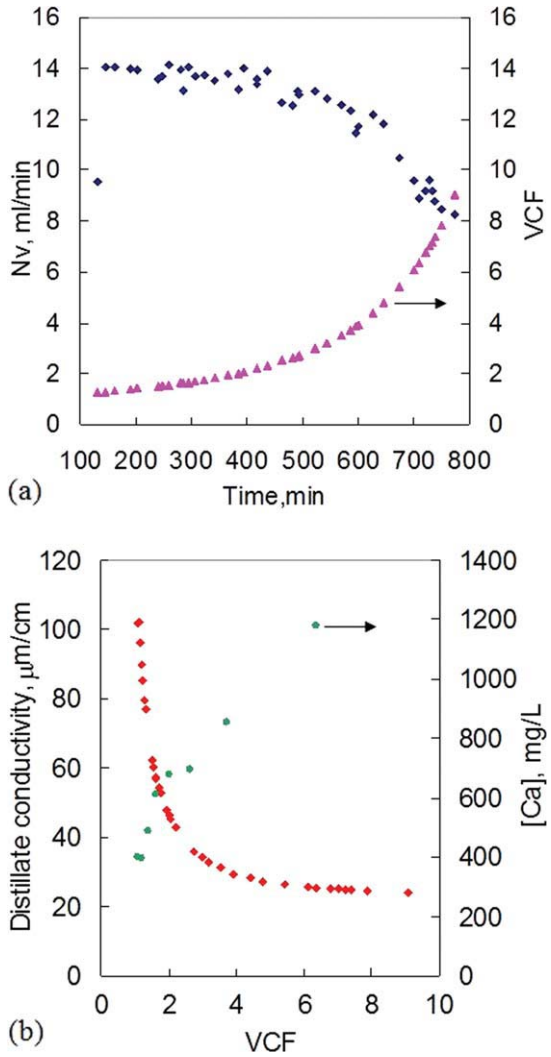

Figure 16. Concentrating artificial sea water with the modified setup of Figure 5b.

(a) Water vapor production rates (N_v) vs. time; (b) distillate conductivities or [Ca] in the brine feed vs. time. The four-stage cascade was used here. Other experimental conditions include: $T_{b,i} = 76°C$, $T_{d,i} = 43°C$, $F_{b,i} = 490$ ml/min, and $F_{d,i} = 490$ ml/min. [Color figure can be viewed in the online issue, which is available at wileyonlinelibrary.com.]

The first trial experiments with artificial sea water containing the scaling salts were conducted with the cascade setup shown in Figure 5a. It was found that a large amount of white deposits covered the heating coil soon after the feed solution was heated up. Because of high local temperature around the electrical heating coil immersed in the feed, calcite precipitated directly onto the heating coil before being fed to the module. Then, membrane fibers were exposed to much lower concentration of calcium ions than that in initial feed, which prevented evaluation of membrane performance with high concentrations of scaling salts. Therefore, the experiment was conducted with the modified setup (Figure 5b) where indirect heating method was applied. The experimental operating conditions were as follows: $T_{b,i} = 76°C$, $T_{d,i} = 43°C$, $F_{b,i} = 490$ ml/min, and $F_{d,i} = 490$ ml/min.

Figure 16a shows the production rate of the water vapor with time and the concentration times of the artificial sea water. After the brine temperature reached a steady temperature of 76°C, the water vapor flux was stable until the artificial sea water was concentrated about three times; beyond this volume concentration factor (VCF = 3), the flux started decreasing slowly. By the time that the artificial sea water was concentrated eight times, the water vapor production rate had declined to 65% of the original steady-state production rate. It is obvious that the increased concentration of the solutes will decrease the vapor pressure of water, which drives the water vapor flux. For example, the values of the vapor pressure for NaCl solutions of 34.4 and 130 salinity at 80°C are 348.5 and 324.5 mm Hg, respectively.[21] In spite of high concentration factor, cleaning the membranes with diluted acid and NaCl solution restored the water vapor flux to more than 95% of the original value.[8,9] It shows that such flux decline due to high concentration factor does not imply irreversible membrane destruction or deformation. It proves the high stability of our DCMD process operation with highly concentrated brines.

Figure 16b shows the distillate conductivity during the membrane distillation process. The distillate conductivity decreased with time as expected because the produced pure water (which was mixed with the original cold distillate) was purer than the initial cold water in the distillate tank. Even when the concentration time reached 8, the distillate conductivity still kept on decreasing.

Figure 16b also illustrates the variation of calcium concentration in the feed with time. With the evaporation of water across the membrane pores, the concentration of calcium ion in the feed increased with time. At around 750 min, the feed solution has been concentrated eight times, but the solution calcium concentration appeared to be concentrated three times. That was because a large amount of crystals deposited onto the membrane module onto the inner wall of the feed tank and also on some other surfaces where the hot feed was passing through, as soon as the supersaturation level was reached (SI > 1) initiating nucleation of calcite, gypsum, etc.

Note that scaling experiments presented in this article were conducted with no intensive pretreatment which RO desalination process requires with such a concentrated feed condition. These experimental results prove the high operational stability of the cross-flow cascade of the fluorosilicone-coated polypropylene hollow fiber membrane modules as reported in Refs. 8–10. Such high stability will benefit both CAPEX and OPEX of the desalination process.

Concluding Remarks

(1) An integrated DCMD-HX process using cross-flow DCMD modules and a solid polymeric hollow fiber-based heat exchanger was successfully developed and experimentally demonstrated.

(2) High values of thermal efficiency, fractional water recovery, and GOR were demonstrated experimentally.

(3) A novel numerical simulator was developed to simulate the performances of a cross-flow DCMD cascade with heat exchange and verified experimentally. The simulations used pure water vapor pressure as the experiments carried out to verify the simulations used tap water. Experiments provided good verification of the simulation.

(4) Modeling results revealed that the highest GOR could be achieved using unequal inlet flow rates of the brine and distillate. The numerical simulator predicts a GOR of 12

when unequal flow rates of the incoming brine and distillate streams are used.

(5) Artificial sea water was concentrated eight times successfully with a countercurrent cascade composed of four stages of the DCMD modules and a heat exchanger, which proves high stability of process even with no intensive pretreatment.

Acknowledgments

The research was sponsored by ONR (Contract No.: N000140510803). This research benefited considerably from the work carried out under a US Bureau of Reclamation Contract for "Pilot-Scale Studies of Direct Contact Membrane Distillation Based Desalination" where a model for the cross-flow DCMD device was developed. The HX was developed in previous ONR contracts (Contract Nos. N00014031102, N000140410810). Jack Gilron spent his sabbatical at NJIT during 09/01/05-08/30/06.

Notation

A_r = area ratio for feed side of fiber (d_o/d_i)
A_{rd} = area ratio for permeate side of fiber (d_i/d_i)
A_{rln} = logarithmic membrane area ratio for fiber (d_{lm}/d_i)
a_M = activity of metal cation
a_X = activity of metal anion
$\bar{a}$ = specific area, $m^2/(m^3/h)$
C_B = concentration of salt in bulk solution
C_P = heat capacity
DCMD = direct contact membrane distillation
D_i = diffusion coefficient of species i
d_i = hollow fiber inner diameter
d_{im} = logarithmic mean diameter of hollow fiber, $(d_o - d_i)/\ln(d_o < d_i)$
d_o = hollow fiber outside diameter
GOR = gained output ratio
h_b = heat transfer coefficient for hot feed brine
h_m = membrane heat transfer coefficient
h_d = heat transfer coefficient on the distillate side
h_{mg} = heat transfer coefficient of the gas phase in the porous membrane
h_{ms} = heat transfer coefficient of the solid phase in the porous membrane
H_0 = reference state specific enthalpy of the brine
i = inlet, ith stage in a cascade, ith module in a multimodule cascade or stage
J = volumetric flux, $m^3/(m^2\ s)$
j = jth stage in a multilayer DCMD module, jth module in a multimodule cascade or stage
k_m = mass transfer coefficient, $kg/(m^2\ h\ Pa)$
K_{sp} = solubility product corresponding to equilibrium solution concentration
K^0_{sp} = thermodynamic solubility product corresponding to equilibrium solution activities
L = length of a hollow fiber
m_m = weight loss of make-up pure water, g
$\dot{m}_{b,i}$ = hot brine flow rate into DCMD unit
$\dot{m}_{b,o}$ = hot brine flow rate out of DCMD unit
$\dot{m}_{d,i}$ = distillate flow rate into DCMD unit
$\dot{m}_{d,o}$ = distillate flow rate out of DCMD unit
$\dot{m}_f$ = fresh brine flow rate
$\dot{m}_{rej}$ = rejected brine flow rate
$\dot{m}_v$ = distillate production rate
n_j = number of fibers in the jth layer
N_v = mass flux of water vapor across the membrane, $kg/(m^2\ s)$
p_{bm} = partial pressure of water vapor at feed membrane interface
p_{dm} = partial pressure of water vapor at permeate membrane interface
Q_{in} = brine water heat duty
$Q(x)$ = rate of heat transfer to membrane at any location
Re = Reynolds number
Sc = Schmidt number
Sh = Sherwood number
SI = saturation index
T = temperature
T_o = reference state temperature
T_b = brine bulk temperature
$T_{b,HX,i}$ = brine temperature entering the heat recovery heat exchanger
$T_{b,HX,o}$ = brine temperature exiting from the heat recovery heat exchanger
$T_{b,i}$ = brine inlet temperature to DCMD
$T_{b,m}$ = brine temperature at the membrane surface
$T_{b,o}$ = brine outlet temperature from DCMD
T_d = distillate bulk temperature
$T_{d,HX,i}$ = distillate temperature entering the heat recovery heat exchanger
$T_{d,HX,o}$ = distillate temperature exiting from the heat recovery heat exchanger
$T_{d,i}$ = distillate inlet temperature to DCMD
$T_{d,m}$ = distillate temperature at the membrane surface
$T_{d,o}$ = distillate outlet temperature from DCMD
T_f = temperature of the fresh brine feed
$V_{b,i}$ = brine inlet flow rate, ml/min
$V_{d,i}$ = distillate inlet flow rate, ml/min
Z = ion charge (algebraic)
$\Delta T_{End} = T_{b,i} - T_{d,o}$
$\Delta T_{stage} = T_{b,i} - T_{b,o}$
$\Delta T_{HX} = T_{d,o} - T_{b,HX,o}$
$\Delta T_{DCMD} = (T_{b,i} - T_{d,o})_{DCMD}$
α = surface area of the distillate in jth stage of cascade per unit length ($n_j \pi d_i$)
η = thermal efficiency
ρ = density
$\gamma_{+/-}$ = mean ionic activity coefficient of calcium sulfate in the supersaturated solution
$\gamma_{+/-,eq}$ = mean ionic activity coefficient of calcium sulfate in the saturated solution
v = represent the stoichiometric coefficients involved in the ionic dissociation process, $v = v_+ + v_-$
ε = membrane porosity

Literature Cited

1. Lawson KW, Lloyd DL. Membrane distillation. *J Membr Sci*. 1997; 124:1–25.
2. Curcio E, Drioli E. Membrane distillation and related operations—a review. *Sep Purif Rev*. 2005;34:35–86.
3. Gilron JL, Song L, Sirkar KK. Design for cascade of cross-flow direct contact membrane distillation. *Ind Eng Chem Res*. 2007;46: 2324–2334.
4. Li B, Sirkar KK. Novel membrane and device for direct contact membrane distillation-based desalination process. *Ind Eng Chem Res*. 2004;43:5300–5309.
5. Li B, Sirkar K. Novel membrane and device for vacuum membrane distillation-based desalination process. *J Membr Sci*. 2005; 257: 60–75.
6. Song L, Li B, Sirkar KK, Gilron JL. Direct contact membrane distillation-based desalination: novel membranes, devices larger-scale studies and a model. *Ind Eng Chem Res*. 2007;46:5300–5309.
7. Song L, Ma Z, Liao X, Kosaraju PB, Irish JR, Sirkar KK. Pilot plant studies of novel membranes and devices for direct contact membrane distillation-based distillation. *J Membr Sci*. 2008;323: 257–270.
8. He F, Gilron J, Lee H, Song L, Sirkar KK. Potential for scaling by sparingly soluble salts in cross-flow DCMD. *J Membr Sci*. 2008; 311:68–80.
9. He F, Sirkar KK, Gilron J. Studies on saling of membranes in desalination by direct contact membrane distillation: $CaCO_3$ and mixed $CaCO_3/CaSO_4$ systems. *Chem Eng Sci*. 2009;64:1844–1859.
10. He F, Sirkar KK, Gilron J. Effects of antiscalants to mitigate membrane scaling by direct contact membrane distillation. *J Membr Sci*. 2009;345:53–58.
11. Schneider K, van Gassel TJ. Membrandestillation. *Chem Ing Tech*. 1984;56:514–521.
12. Fane AG, Schofield RW, Fell CJD. The efficient use of energy in membrane distillation. *Desalination*. 1987;64:231–243.

13. Alkali AM, Lior N. Membrane-distillation desalination: status and potential. *Desalination*. 2004;171:111–131.
14. Zukauskas A. *Heat transfer from tubes in cross flow*. In: Hartnett JP, Irvine TF Jr, editors. *Advances in Heat Transfer*, Vol.8. New York: Academic Press, 1972, 93–160.
15. Zarkadas DM, Sirkar KK. Polymeric hollow fiber heat exchangers: an alternative for lower temperature applications. *Ind Eng Chem Res*. 2004;43:8093–8106.
16. Gryta M, Tomaszewska M. Heat transport in the membrane distillation process. *J Membr Sci*. 1998;144:211–222.
17. Gostoli C, Matulli S, Sarti GC. Low temperature distillation through hydrophobic membranes. *Sep Sci Technol*. 1987;22:855–872.
18. Sarti GC, Gostoli C, Matulli S. Low energy cost desalination processes using hydrophobic membranes. *Desalination*. 1985;56:277–286.
19. Bajt O, Sket B, Faganeli J. The aqueous photochemical transformation of acrylic acid. *Marine Chem*. 1997;58:255–259.
20. Meijer JAM, Rosemalen GMV. Solubilities and supersaturations of calcium sulfate and its hydrates in seawater. *Desalination*. 1984;51:255–305.
21. Fabuss BM. *Properties of sea water*. In: Spiegler KS,Laird ADK, editors. *Principles of Desalination Part B*, 2nd ed. New York: Academic Press, 1980:765–799.

Manuscript received Sept. 25, 2009, and revision received July 29, 2010.